Human Molecular Genetics, 2022, Vol. 31, No. 5 718–732

https://doi.org/10.1093/hmg/ddab276
Advance Access Publication Date: 28 September 2021
General Article

GENERAL ARTICLE

Sarcospan increases laminin-binding capacity of α-dystroglycan to ameliorate DMD independent of *Galgt2*

Hafsa Mamsa[1,†], Rachelle L. Stark[1,‡], Kara M. Shin[1,‡], Aaron M. Beedle[2] and Rachelle H. Crosbie[1,3,4,5,*]

[1]Department of Integrative Biology & Physiology, University of California, Los Angeles 90095, USA, [2]Department of Pharmaceutical Sciences, Binghamton University State University of New York, New York 13902, USA, [3]Broad Stem Cell Institute, University of California, Los Angeles 90095, USA, [4]Department of Neurology, David Geffen School of Medicine, University of California, Los Angeles 90095, USA and [5]Molecular Biology Institute, University of California, Los Angeles 90095, USA

*To whom Correspondence should be at: University of California Los Angeles, Department of Integrative Biology & Physiology, 610 Charles E. Young Drive East, Terasaki Life Science Building, Los Angeles, CA 90095, USA. Tel: 310-794-2103; Email: rcrosbie@physci. ucla.edu

Abstract

In Duchenne muscular dystrophy (DMD), mutations in dystrophin result in a loss of the dystrophin-glycoprotein complex (DGC) at the myofiber membrane, which functions to connect the extracellular matrix with the intracellular actin cytoskeleton. The dystroglycan subcomplex interacts with dystrophin and spans the sarcolemma where its extensive carbohydrates (matriglycan and CT2 glycan) directly interact with the extracellular matrix. In the current manuscript, we show that sarcospan overexpression enhances the laminin-binding capacity of dystroglycan in DMD muscle by increasing matriglycan glycosylation of α-dystroglycan. Furthermore, we find that this modification is not affected by loss of *Galgt2*, a glycotransferase, which catalyzes the CT2 glycan. Our findings reveal that the matriglycan carbohydrates, and not the CT2 glycan, are necessary for sarcospan-mediated amelioration of DMD. Overexpression of *Galgt2* in the DMD *mdx* murine model prevents muscle pathology by increasing CT2 modified α-dystroglycan. *Galgt2* also increases expression of utrophin, which compensates for the loss of dystrophin in DMD muscle. We found that combined loss of *Galgt2* and dystrophin reduced utrophin expression; however, it did not interfere with sarcospan rescue of disease. These data reveal a partial dependence of sarcospan on *Galgt2* for utrophin upregulation. In addition, sarcospan alters the cross-talk between the adhesion complexes by decreasing the association of integrin β1D with dystroglycan complexes. In conclusion, sarcospan functions to re-wire the cell to matrix connections by strengthening the cellular adhesion and signaling, which, in turn, increases the resilience of the myofiber membrane.

[†]Hafsa Mamsa, http://orcid.org/0000-0002-0879-6635
[‡]These authors contributed equally.

Received: September 30, 2020. **Revised:** August 27, 2021. **Accepted:** September 13, 2021

Introduction

Duchenne muscular dystrophy (DMD) is an X-linked disorder caused by mutations in the DMD gene (1), resulting in the loss of the dystrophin protein. DMD is the most common fatal disease in children, affecting 1 in approximately 5700 boys (2) and is characterized by early onset progressive muscle weakness and muscle wasting leading to loss of ambulation, respiratory impairment, and cardiomyopathy. Dystrophin is a component of the DGC composed of integral and peripheral membrane proteins (3–7). The DGC functions as a receptor for ligands in the extracellular matrix (ECM) and protects the sarcolemma from contraction induced injury by connecting the actin cytoskeleton (8) to the ECM. Loss of dystrophin in DMD reduces expression of the DGC complex from the muscle cell membrane or sarcolemma (3,4). Loss in maintaining this physical connection compromises membrane integrity resulting in contraction induced membrane damage (9,10), calcium dysregulation, inflammation, and asynchronous cycles of degeneration and regeneration leading to fibrosis and adipose tissue accumulation. The DGC is composed of dystrophin, α- and β-dystroglycan (α-DG and β-DG), and the sarcoglycan-sarcospan subcomplex (SG-SSPN). There are two additional adhesion complexes in skeletal muscle with overlapping function with the DGC: the utrophin-glycoprotein complex (UGC) and $\alpha7\beta1$ integrin (11–14). The UGC is similar to the DGC, with a key distinction that dystrophin is replaced by utrophin, a autosomal paralogue of dystrophin with similar structure and function (11,15,16).

SSPN is an integral membrane protein of the DGC and UGC and also associates with the integrin complex (17–21). We have previously shown that transgenic overexpression of SSPN in *mdx* mice, a murine model of DMD, increased the abundance of the UGC and $\alpha7\beta1$ integrin at the myofiber membrane, increased CT2 glycosylation of α-DG, and enhanced laminin binding (20–22). SSPN overexpression improved dystrophic pathology by increasing membrane stability, which improved muscle function with post-exercise activity levels and eccentric contraction induced force production to near wild-type levels (22). SSPN upregulation also had beneficial effects on pulmonary and cardiac muscle physiology (22–24).

Similar to utrophin and SSPN, the ectopic overexpression of the glycosyltransferase *Galgt2* in *mdx* mice caused several proteins (UGC, agrin, α4- and α5-laminin), normally confined to the neuromuscular junction (NMJ) and myotendinous junction (MTJ), to be redistributed to the extrasynaptic sarcolemma, leading to amelioration of skeletal and cardiac muscle disease (25–27). *Galgt2* (B4*Galnt2*) encodes a type II Golgi transmembrane protein that catalyzes the addition of a terminal β1,4-linked N-acetylgalactosamine (β1,4GalNAc) sugar moiety onto the cytotoxic T-cell (CT) glycan of select glycoproteins and glycolipids, creating the CT2 glycan [GalNAcβ1–4[Neu5Gcα2–3]Galβ1–4GlcNAcβ-] (28). GALGT2 is expressed throughout the sarcolemma during development and regeneration, however, it is restricted to the post-synaptic NMJ and the MTJ in adult muscle (25,26,29). Employing a targeted approach, α-DG was identified as a substrate for GALGT2 (25) and CT glycosylation of α-DG improved its laminin-binding capacity (30). Interestingly, overexpression of SSPN increased CT2-modified α-DG in muscle lysates, likely caused by the increased abundance of endogenous GALGT2 in ER/Golgi vesicle preparations from *mdx*: SSPN-Tg skeletal muscle (21). This suggested that SSPN may increase CT2 modified α-DG through regulating GALGT2 production, which raised the questions of whether SSPN and GALGT2 are members of a shared or redundant pathway and whether GALGT2 expression is required for SSPN mediated protection of *mdx* muscle. To address these questions, we investigated the dependency of SSPN on GALGT2 in the amelioration of dystrophin deficiency in *mdx* disease.

Results

SSPN improves DMD histopathology in *mdx* muscle in the absence of GALGT2

To determine if loss of GALGT2 affects the therapeutic function of SSPN in dystrophin-deficient *mdx* mice, we generated SSPN-transgenic (Tg) mice lacking: 1) dystrophin (*mdx* ^{Tg}) and 2) both dystrophin and *Galgt2* (dko^{Tg}), as outlined in Figure 1A. As expected, *mdx* mice exhibit increased body weight relative to wild-type controls due to muscle hypertrophy and hyperplasia, while loss of GALGT2 in *mdx* mice did not affect body weight (Fig. 1B, Supplementary Material, Fig. S1) (29,31,32). We found that *mdx*^{Tg} and dko^{Tg} weighed significant less than non-transgenic littermates (Fig. 1B, Supplementary Material, Fig. S1), prompting an evaluation of cross-sectional area (CSA) of individual muscle fibers. CSA analysis revealed that, similar to *mdx*, dko mice displayed considerable heterogeneity in fiber area due to chronic degeneration and regeneration with a peak fiber diameter of 500 μm^2 with smaller newly regenerated and larger hypertrophic fibers resulting in an average fiber diameter of 2200–2250 μm^2 (Fig. 1C) (29). The remarkable reduction in fiber size variation and a shift in peak CSA to larger fibers (1000 μm^2) and average fiber diameter of 1200–1400 μm^2 in SSPN overexpressing muscle suggests that the decrease in regeneration mediated by SSPN is not affected by deletion of *Galgt2* (Fig. 1C).

Histological analysis of transverse quadriceps sections stained with hematoxylin and eosin (H&E) reveals that centrally located nuclei, a marker of myofiber regeneration, although abundant in *mdx* and dko muscles, were markedly reduced by SSPN-Tg such that the central nucleation values of dko^{Tg} muscle were indistinguishable from *mdx*^{Tg} (Fig. 1D and E). While centrally located nuclei persist for over a month, embryonic myosin heavy chain (eMHC) is a short-lived maker for newly regenerating myofibers. We observed a trend of reduced eMHC positive myofibers in *mdx*^{Tg} and dko^{Tg} skeletal muscle compared to *mdx* and dko littermates (Fig. 1D and F). These trends are consistent with the number of myofibers with central nucleation and reveal marked reduction in regeneration with SSPN overexpression. To determine whether diminished regenerative capacity could lead to a reduction in the ability to form new myofibers in skeletal muscle overexpressing SSPN, we assessed levels of Pax7 positive satellite cells, a marker for adult muscle stem cells, by immunofluorescence analysis. The density of Pax7 positive satellites cells in quadricep muscles from *mdx*^{Tg} and dko^{Tg} were similar to that for wild-type controls demonstrating similar regenerative potential (Fig. 1G). Taken together, these data suggest that SSPN mediated amelioration of dystrophic pathology is independent of *Galgt2* expression in *mdx* mice.

SSPN increases expression of mature α-DG at the sarcolemma in the absence of GALGT2

Although increased expression of the UGC at the extrasynaptic *mdx* sarcolemma has been documented in Galgt2-Tg *mdx* muscle, it is unknown how combined loss of dystrophin and GALGT2 affects membrane expression of the adhesion complexes. To evaluate the consequence of GALGT2 deficiency

A

Genotype	Description	Abbreviation
***mdx* : *Galgt2* $^{+/+}$: SSPN-non-Tg**	dystrophin-deficient mouse model for DMD	*mdx*
***mdx* : *Galgt2* $^{-/-}$: SSPN-non-Tg**	*mdx* mice lacking *Galgt2*	dko
***mdx* : *Galgt2* $^{+/+}$: SSPN-Tg**	*mdx* mice overexpressing the human SSPN transgene	*mdx*^{Tg}
***mdx* : *Galgt2* $^{-/-}$: SSPN-Tg**	*mdx* mice lacking *Galgt2* and overexpressing the human SSPN transgene	dko^{Tg}

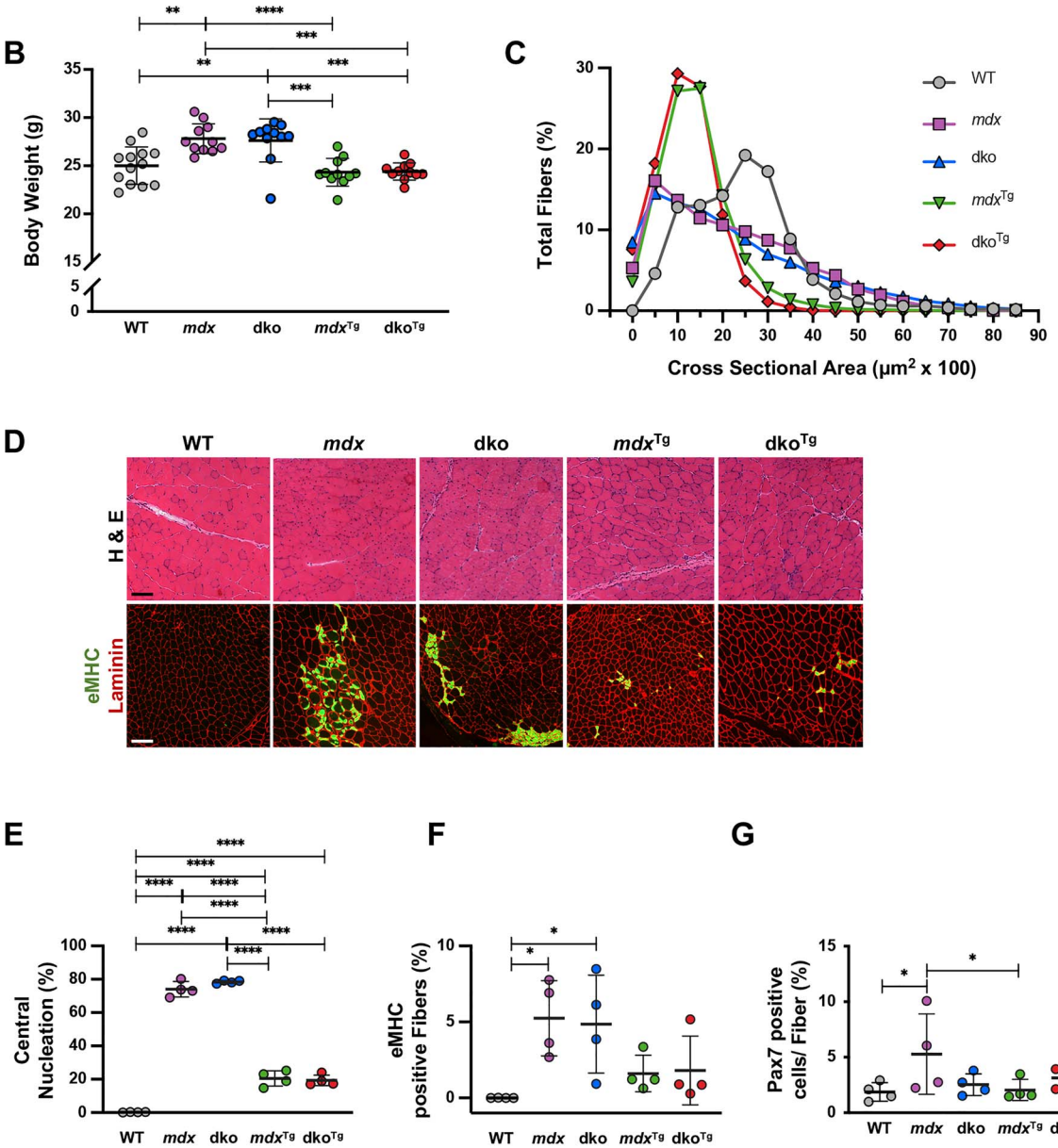

Figure 1. Sarcospan-mediated amelioration of muscle pathology does not require GALGT2. (**A**) *mdx:Galgt2* $^{+/-}$ mice were crossed with *mdx:Galgt2*$^{+/-}$:SSPN-Tg to generate the listed genotypes that were included in the study. (**B**) Body weight among the five mouse lines for males 10–11.5 week old. Statistical analysis was performed by two-way ANOVA with Tukey's multiple comparison tests (n = 11–13 biological replicates per genotype). (**C**) Distribution of cross-sectional areas of individual muscle fibers of mouse quadriceps 10–12-week old. Data were binned per 500 μm^2. (**D**) Representative transverse cryosections of quadriceps muscles stained with hematoxylin and eosin (H&E) reveals that there are no robust differences in histopathology in *mdx*:SSPN-Tg mice in the presence or absence of GALGT2. Scale bar, 50 μm. Immunofluorescence analysis of embryonic myosin heavy chain (eMHC; green) on transverse quadricep sections showing newly regenerated fibers. Muscle sections are co-stained with antibodies to laminin (red) to denote individual muscle fibers. Scale bar, 500 μm. (**E**) Quantification of centrally located nuclei, a marker of muscle regeneration from H&E-stained quadriceps cryosections. Statistical analysis was performed by one-way ANOVA with Tukey's multiple comparison tests (n = 4 biological replicates per genotype). (**F**) Quantification of percent positive eMHC fibers. Statistical analysis was performed using one-way ANOVA with Tukey's multiple comparison tests (n = 4 biological replicates per genotype). (**G**) Quantification of Pax7 positive cells per myofiber (percent). Statistical analysis was performed using one-way ANOVA with Dunn's multiple comparison test (n = 4 biological replicates per genotype). Tissues used in C-G were quadriceps from 10–13 week old males. All data represented as mean +/− standard deviation (*$P < 0.05$, **$P < 0.01$, ***$P < 0.001$ and ****$P < 0.0001$).

in SSPN-mediated upregulation of adhesion complex proteins at the membrane, we performed indirect immunofluorescence on transverse quadriceps sections. Since loss of GALGT2 most notably affects the levels of WFA reactive α-DG in dystrophin-deficient muscle lysates, we first looked for changes in the sarcolemmal expression of α-DG. We did not observe any significant differences in the membrane expression of either the core α-DG polypeptide, detected using an antibody that recognizes all forms of α-DG, or the mature glycosylated α-DG (α-DG^{IIH6}), detected with carbohydrate-specific antibodies IIH6, between *mdx* and dko muscle (Fig. 2A). α-DG is extensively glycosylated via O-mannosylation and these carbohydrate moieties, referred to as matriglycan, are the primary binding site for ECM ligands (33–35). Improper maturation of α-DG disrupts binding to ligands in the ECM leading to a concomitant reduction of cellular adhesion (36,37). However, overexpression of SSPN dramatically increases the abundance of mature glycosylated α-DG (α-DG^{IIH6}) at the sarcolemma relative to wild-type (Fig. 2A). While expression of the core protein in *mdx*^{Tg} is elevated compared to *mdx*, it is not restored to wild-type levels (Fig. 2A). The increase in α-DG core polypeptide was not affected by the absence of GALGT2 (Fig. 2A). These data suggest that SSPN influences the O-mannosyl oligosaccharide decoration of α-DG by either increasing the number of IIH6 epitopes and/or altering the structure of α-DG such that the IIH6 binding site becomes more accessible to antibodies.

Since we did not observe differences in the membrane expression of α-DG in GALGT2-deficient muscle, we next examined WFA binding, reasoning that reduced CT2 glycosylation may manifest as lower abundance of WFA in lectin overlays. In normal muscle, WFA is concentrated at the post-synaptic sarcolemma at the NMJ; however, it decorates the entire sarcolemma of *mdx* myofibers (Fig. 2A). Surprisingly, this binding was not altered in the absence of GALGT2 in dko muscle (Fig. 2A). We have previously shown that increasing levels of SSPN resulted in a concomitant increase in WFA binding in a SSPN dose-dependent fashion (21). Furthermore, we find that the WFA binding is not disrupted by loss of GALGT2 activity in the dko^{Tg} samples (Fig. 2A). Although WFA interacts with CT2 carbohydrates on α-DG, it indiscriminately recognizes other terminal βGalNAc molecules as well that are present on other proteins or lipids, such as those with chondroitin sulfate glycosylaminoglycan chains (26,38–41).

SSPN enhances modification of α-DG with laminin-binding matriglycan regardless of GALGT2

Based on the observation that SSPN influenced expression of mature α-DG at the cell surface (Fig. 2A), we further investigated the glycosylation of α-DG using *Wisteria Floribunda* agglutinin (WFA) or succinylated wheat germ agglutinin (sWGA) lectin enrichments of skeletal muscle lysates solubilized with digitonin, a mild non-ionic detergent that is known to preserve the protein–protein interactions within the DGC and UGC (6). Bound glycoproteins were eluted with buffers containing GalNAc for WFA or GlcNAc for sWGA and immunoblotted for adhesion complex proteins. Analysis of total protein lysates displayed highest expression of α-DG in wild-type followed by SSPN-Tg samples and lowest expression in *mdx* and dko muscle (Fig. 2B). Interestingly, contrary to published data showing drastically reduced levels of glycosylated α-DG ^{IIH6} in WFA fractions in dko muscle, we did not observe any significant differences in WFA associated α-DG^{IIH6} in muscle homogenates from dko relative to *mdx* samples (Fig. 2C and D). Furthermore, the dramatic increase in α-DG^{IIH6} observed with SSPN overexpression in *mdx* was not impacted by the absence of GALGT2. We next immunoblotted WFA eluates with the antibodies that recognize the core α-DG polypeptide. We found that abundance of fully glycosylated α-DG polypeptide (>130 kDa) was similar between wild-type, *mdx*, and dko samples, however, was significantly increased in both SSPN-Tg samples (Fig. 2C and D). We also observed a smaller, hypoglycosylated form of α-DG (>100 kDa, ∗ asterik) in the WFA eluates that was not cross-reactive with IIH6 antibodies. Interestingly, the abundance of immature α-DG decreased in the SSPN-Tg samples (Fig. 2C), supporting the conclusion that SSPN shifted α-DG from an immature to a fully mature form with matriglycan carbohydrates that enable laminin interaction. This finding was specific to WFA binding complexes as we did not observe these changes in sWGA eluates (Fig. S2). Interestingly, we did observe a hyperglycosylated form of α-DG (>225 kDa) in both WFA and sWGA eluates from SSPN-Tg samples (Fig. 2C, Supplementary Material, Fig. S2, arrowhead). Taken together with the sarcolemmal expression of α-DG, these data suggest that SSPN influences the maturation of the O-mannosyl moiety of α-DG, elevates the level of mature α-DG^{IIH6} and may also affect the accessibility of the matriglycan structure at the myofiber membrane.

The increased sarcolemmal expression and maturation of α-DG prompted us to examine the levels of β-DG and additional adhesion complex members. α-DG, on the extracellular face, is anchored to the sarcolemma by associating with β-DG, which interacts directly with either dystrophin or utrophin (8,42,43). We found that β-DG expression at the sarcolemma resembles that of the core α-DG for all genotypes (Fig. 2A). Similar to *mdx*, β-DG is dramatically reduced at the sarcolemma in dko skeletal muscle relative to wild-type (Fig. 2A). Increased β-DG expression was maintained in SSPN-Tg muscle relative to *mdx* and dko regardless of GALGT2 expression (Fig. 2A). Like α-DG, the binding of β-DG in WFA precipitations in dko skeletal muscle relative to *mdx* are similar (Fig. 2 C and D). Deletion of *Galgt2* did not influence the SSPN mediated increases in β-DG in WFA complexes (Fig. 2 C and D). We did observe an increase in modification of β-DG in the SSPN-Tg samples, as revealed by a 2 kDa upward shift in MW, which likely reflects an increase in N-linked glycosylation of β-DG.

GALGT2 is not required for membrane localization of the sarcoglycans

The DGs are further stabilized to the membrane through association with the SG-SSPN subcomplex (18,19,44). We investigated the sarcolemma expression of the four skeletal muscle SGs. As expected, the SGs were highly expressed at the sarcolemma in wild-type muscle, which was diminished in *mdx* samples and robustly increased in *mdx* ^{Tg} muscle (Fig. 3A). Loss of GALGT2 did not affect the levels of the SGs at the sarcolemma in dystrophic muscle (*mdx* vs. dko) nor in the SSPN-Tg samples (*mdx*^{Tg} vs. dko^{Tg}). The interaction of SSPN with the SGs to form the SG-SSPN subcomplex is highly resistant to pH and detergent dissociation (18). Anchored to the membrane by four transmembrane domains, SSPN also contains an extracellular loop with residues that interact with the SGs and β-DG (17,45). As expected, SSPN transgenic lines display abundant expression of SSPN, which was greatly reduced in *mdx* and dko myofiber membrane (Fig. 3A). Analysis of the WFA eluates revealed significantly elevated levels of β-SG in dystrophic mice in the absence of GALGT2 (*mdx* vs dko), without affecting incorporation of γ-SG

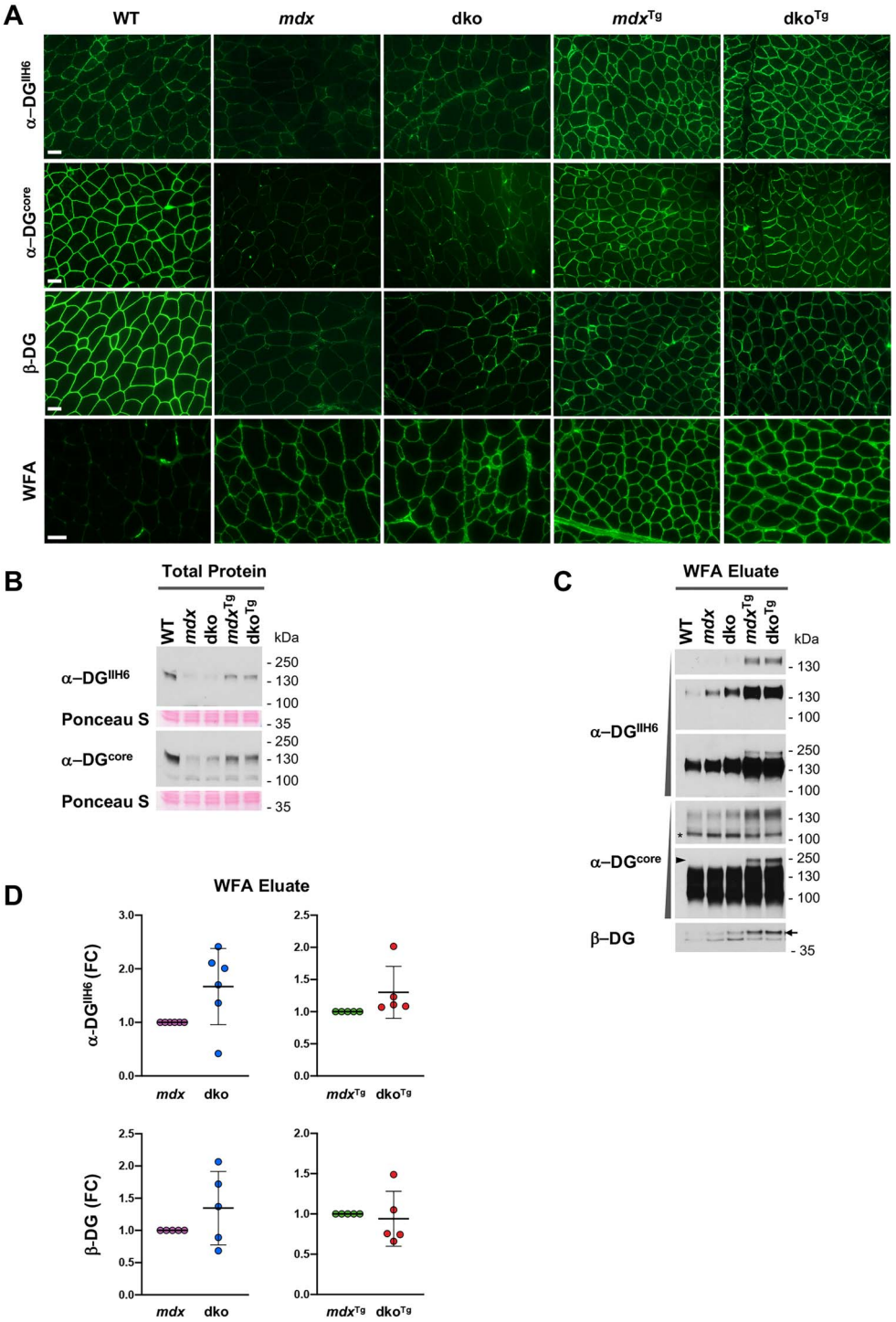

Figure 2. Sarcospan elevates WFA reactive mature α- dystroglycan ^{IIH6} at the sarcolemma regardless of GALGT2. (**A**) Immunofluorescence analysis of transverse quadriceps cryosections of wild-type (WT), *mdx*, *mdx*:*Galgt2*$^{-/-}$ (dko), *mdx*:SSPN-Tg (*mdx*^{Tg}), *mdx*:*Galgt2*$^{-/-}$:SSPN-Tg (dko^{Tg}) with antibodies against laminin-binding glycoepitope of α-dystroglycan (α-DG^{IIH6}) or the polypeptide protein core of α-dystroglycan (α-DG^{core}) and β-dystroglycan (β-DG). Scale bar, 50 μm. (**B**) Total skeletal muscle lysates immunoblotted for the indicated antigens. Ponceau S is shown as protein loading control. (**C**) Skeletal muscle lysates enriched with WFA immunoblotted for the indicated antigens and quantification of data by densitometry in (C). Exposure level high to low displayed by left triangle. Arrowhead indicates hyperglycosylated form of α-DG and asterisk (*) denotes the discrete hypoglycosylated band. Arrow marks glycosylated form of β-DG. Fold change (FC) shown for dko relative to *mdx* and dko^{Tg} relative to *mdx*^{Tg}. All data represented as mean +/− standard deviation. Statistical analysis was performed using Welch's *t*-test (n = 5–6 biological replicates per genotype).

(Fig. 3B and C). Taken together with the relatively similar expression of β-SG at the dko and *mdx* sarcolemma, these data suggest that there may be a compensatory increase in incorporation of β-SG in WFA complexes in the absence of GALGT2 which did not affect the expression at the sarcolemma. The elevated levels of β-SG and γ-SG in WFA complexes in SSPN transgenic

muscle lysates were not impacted by the absence of GALGT2 (Fig. 3B and C). SSPN-Tg associated with the WFA complex at similar levels, regardless of GALGT2 expression (Fig. 3B).

Loss of GALGT2 reduces utrophin, but not integrin, upregulation by SSPN

Indirect immunofluorescence analysis of muscle cryosections confirms abundant dystrophin expression at the sarcolemma (Fig. 4A) and in WFA-associated complexes (Fig. 4B) in wild-type muscle and its absence from dystrophin-deficient muscle. Utrophin and dystrophin are co-expressed and enriched at the NMJ and MTJ (46,47), where they associate with β-DG (11). As expected, we find that utrophin is restricted to the neuromuscular junction in wild-type muscle and surrounds the myofiber in *mdx* and dko (Fig. 4A). SSPN-Tg induces enhanced extrasynaptic utrophin expression (Fig. 4A), which is reduced in the absence of GALGT2 (Fig. 4A). This suggests that loss of GALGT2 negatively impacts SSPN's ability to fully restore utrophin at the sarcolemma. Furthermore, lectin enrichments revealed a trend for decreased WFA-associated utrophin in the absence of GALGT2 in dko^{Tg} relative to *mdx*^{Tg} genotypes (Fig. 4B and C). We have previously shown that SSPN amelioration of *mdx* pathology is dependent on utrophin and $\alpha 7$ integrin expression (48). Integrin complexes are composed of heteromeric α and β subunits, with $\alpha 7\beta 1$ integrin being the major integrin species in adult muscle and is part of a native compensatory response in dystrophin-deficiency (49,50). We did not observe significant differences in the sarcolemma expression of ITGB1 in the SSPN overexpression models or in the absence of GALGT2 (data not shown). Analysis of total homogenates confirms very low levels of ITGB1 in wild-type muscle, increased expression in *mdx* and dko and greatest levels in *mdx*^{Tg} and dko^{Tg} (Fig. 4D). We observed this trend for both the mature and precursor forms of ITGB1. In contrast, levels of ITGB1 associated with WFA complexes were reduced in *mdx*^{Tg} and dko^{Tg} relative to *mdx* and dko (Fig. 4B and C). Taken together, these data suggest that there may be more integrin complexes that are independent of DG in SSPN-Tg muscle. It also points to a dynamic role for integrins, in which SPPN may be interacting with integrins at focal adhesions and recycling of integrin complexes to mediate cellular signaling.

SSPN overexpression enhances the laminin-binding capacity in the absence of GALGT2

Given that transgenic overexpression of SSPN increases two laminin receptors (matriglycan decorated α-DG^{IIH6} and integrin $\alpha 7\beta 1$) and that CT2 glycosylation of α-DG improves laminin binding (30), we next evaluated how loss of GALGT2 would affect laminin's interaction with α-DG. We employed a solid-phase laminin-binding assay (36) to assess the relative binding capacity of purified laminin-111 to WFA enrichments from quadriceps muscles immobilized on microtiter plate. WFA enrichments form *mdx*^{Tg} and dko^{Tg} muscle exhibited significantly enhanced laminin binding compared to WT, *mdx* and dko samples (Fig. 5A). To more specifically test for interaction between laminin and α-DG, we next performed a solid-phase α-DG binding assay in which WFA enrichments were bound to immobilized laminin-111 and detected using core α-DG polypeptide specific antibodies. Consistent with the solid-phase laminin-binding assay, we observed reduced binding of α-DG to laminin-111 in WFA enrichments from WT, *mdx* and dko relative to *mdx*^{Tg} and dko^{Tg} WFA eluates (Fig. 5B). Furthermore, these data directly correlated with the levels of mature α-DG^{IIH6} levels in our WFA enrichments (Fig. 5C). Immunoblotting also confirm relatively similar levels of SSPN-Tg in solubilized muscle from *mdx*^{Tg} and dko^{Tg} (Fig. 5D). While we have solubilized skeletal muscle using a RIPA buffer containing ionic detergents for these assays, it may be insufficient to disrupt all protein–protein interactions within the adhesion complexes and additional laminin-binding receptors may partially co-enrich. Indeed, low levels of integrin β1D co-precipitated with α-DG^{IIH6} in WFA enrichments (Fig. 5C). As the WFA enrichments contain both mature and hypoglycosylated forms of α-DG, we investigated the binding of laminin to the mature α-DG^{IIH6} by performing laminin overlay on denatured WFA enrichments immobilized by SDS-PAGE. These data support the solid-phase binding assays and demonstrate that while laminin binds to the mature α-DG^{IIH6} (arrowhead), it does not interact with the hypoglycosylated fraction of α-DG (Fig. 5C, Supplementary Material, Fig. S2; $*$ asterik).

SSPN protects the sarcolemma from membrane injury in the absence of GALGT2

Loss of the DGC leads to muscle membrane instability and susceptibility to contraction induced muscle tears that permit an unregulated exchange of materials with the blood, including infiltration of circulating IgG and IgM (51). Immunofluorescence staining of IgG antibodies in transverse quadriceps sections shows significantly more IgG positive fibers in *mdx* compared to all other genotypes (Fig. 6A and B). Overexpression of SSPN has been shown to reduce membrane fragility under dystrophin deficiency (20–24). Interestingly, loss of GALGT2 significantly reduced IgG uptake into myofibers in *mdx* muscle (*mdx* vs. dko) and SSPN-Tg rescues membrane instability regardless of GALGT2 (Fig. 6A and B).

We next sought to understand if improved muscle integrity and the enhanced laminin binding correlated with levels of laminin at the sarcolemma. Here, we show that loss of GALGT2 does not affect the level of laminin immunostaining in the basement membrane (Fig. 6C). Consistent with elevated levels of mature α-DG^{IIH6} in the *mdx*^{Tg} and dko^{Tg} sarcolemma, a receptor for laminin, there is a concomitant increase in laminin at the basement membrane, which is unaffected by the genetic ablation of GALGT2.

Discussion

With the eventual goal of developing a therapy for DMD, several studies are harnessing the natural compensatory upregulation of utrophin or $\alpha 7\beta 1$ integrin in *mdx* as a mechanism to improve outcomes of DMD (12–14,49,52). That these proteins, like GALGT2 and SSPN, impart therapeutic effects, ultimately by increasing laminin-binding complexes to the myofiber membrane, highlight the crucial function of restoring cell to matrix connection. Currently, we are pursuing pharmacological upregulation of SSPN as a potential clinical therapy for DMD and related dystrophies (53). To understand the mechanism by which SSPN compensates for dystrophin loss, we have previously generated independent murine models: *mdx:utrn*$^{-/-}$:SSPN-Tg, *mdx:Itga7*$^{-/-}$:SSPN-Tg and *Large*^{myd}:SSPN-Tg (like-glycotransferase; an enzyme critical for generating the matriglycan laminin-binding epitope on α-DG) (21,48). Our findings are presented in Fig 6D. In the present study, we assessed the contribution of GALGT2 in SSPN mediated rescue of dystrophic pathology.

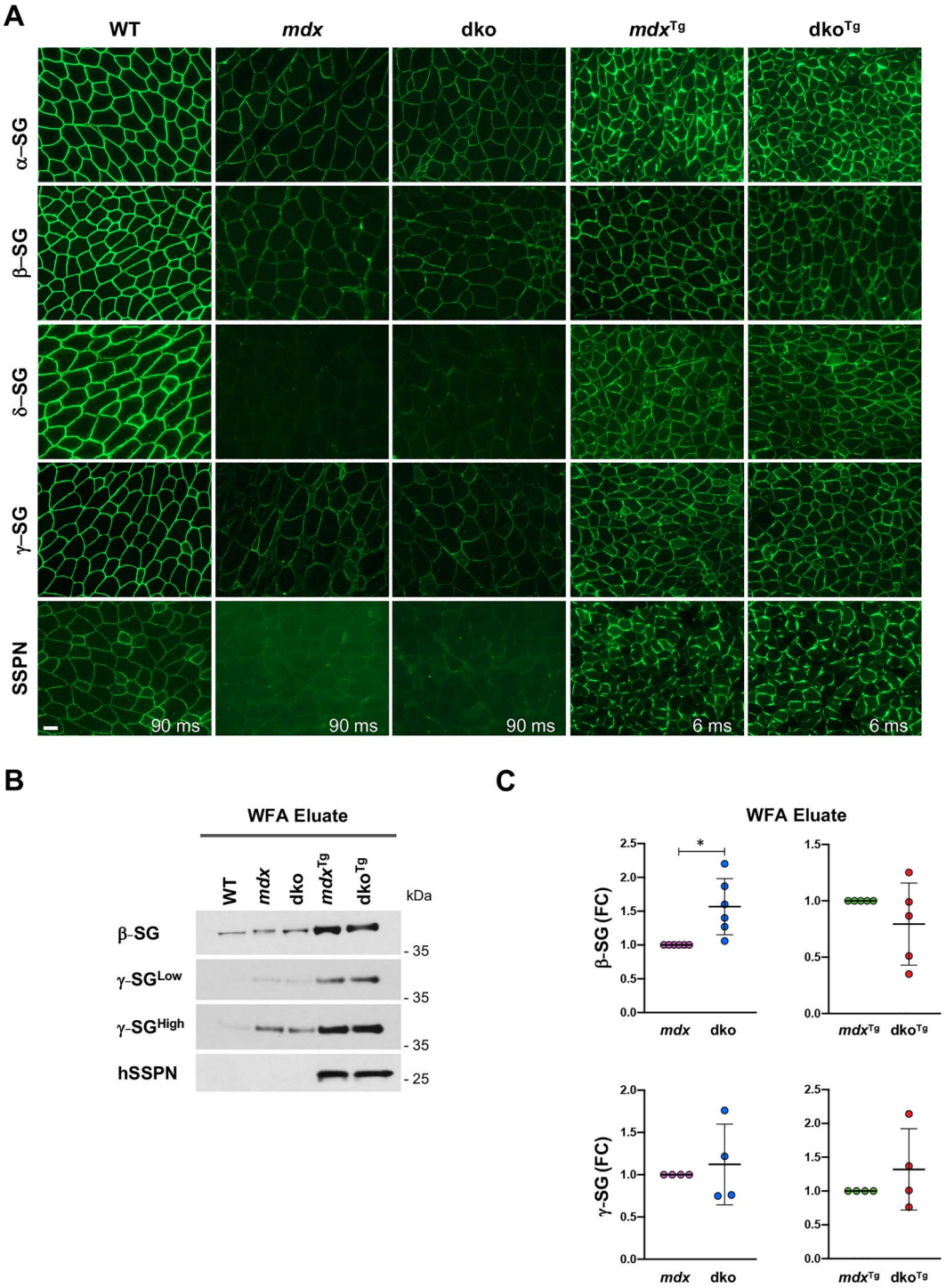

Figure 3. Loss of GALGT2 influences β-sarcoglycan association with WFA binding adhesion complexes in *mdx*:*Galgt2*$^{-/-}$ muscle. (**A**) Immunofluorescence analysis of transverse quadriceps cryosections of WT, *mdx*, *mdx*:*Galgt2*$^{-/-}$ (dko), *mdx*:SSPN-Tg (*mdx*^{Tg}), *mdx*:*Galgt2*$^{-/-}$:SSPN-Tg (dko^{Tg}) with the indicated antibodies. Scale bar, 50 μm. (**B**) Skeletal muscle lysates enriched with WFA immunoblotted for indicated antigens with quantification data by densitometry in (**C**). Exposure levels indicated (high and low) for γ-SG. Fold change (FC) shown for dko relative to *mdx* and dko^{Tg} relative to *mdx*^{Tg}. All data represented as mean +/− standard deviation. Statistical analysis was performed using Welch's *t*-test (n = 4–6 biological replicates per genotype; $^{*}P < 0.05$). α-sarcoglycan (α-SG), β-sarcoglycan (β-SG), δ-sarcoglycan (δ-SG), γ-sarcoglycan (γ-SG), human sarcospan (hSSPN).

We report nuanced changes in the composition of the WFA reactive adhesion complex in dko muscles relative to *mdx*, which did not affect their sarcolemmal expression. The differences in WFA reactive α-DG ^{IIH6} levels between our study and published data can be attributed to several factors. Xu and colleagues reported that WFA reactive α-DG is greatly diminished, however not entirely abolished, in dko muscle solubilized with NP-40 (29), which may indicate the presence of additional glycotransferases that may at least partially compensate for loss of GALGT2. In order to retain protein–protein interactions within the adhesion

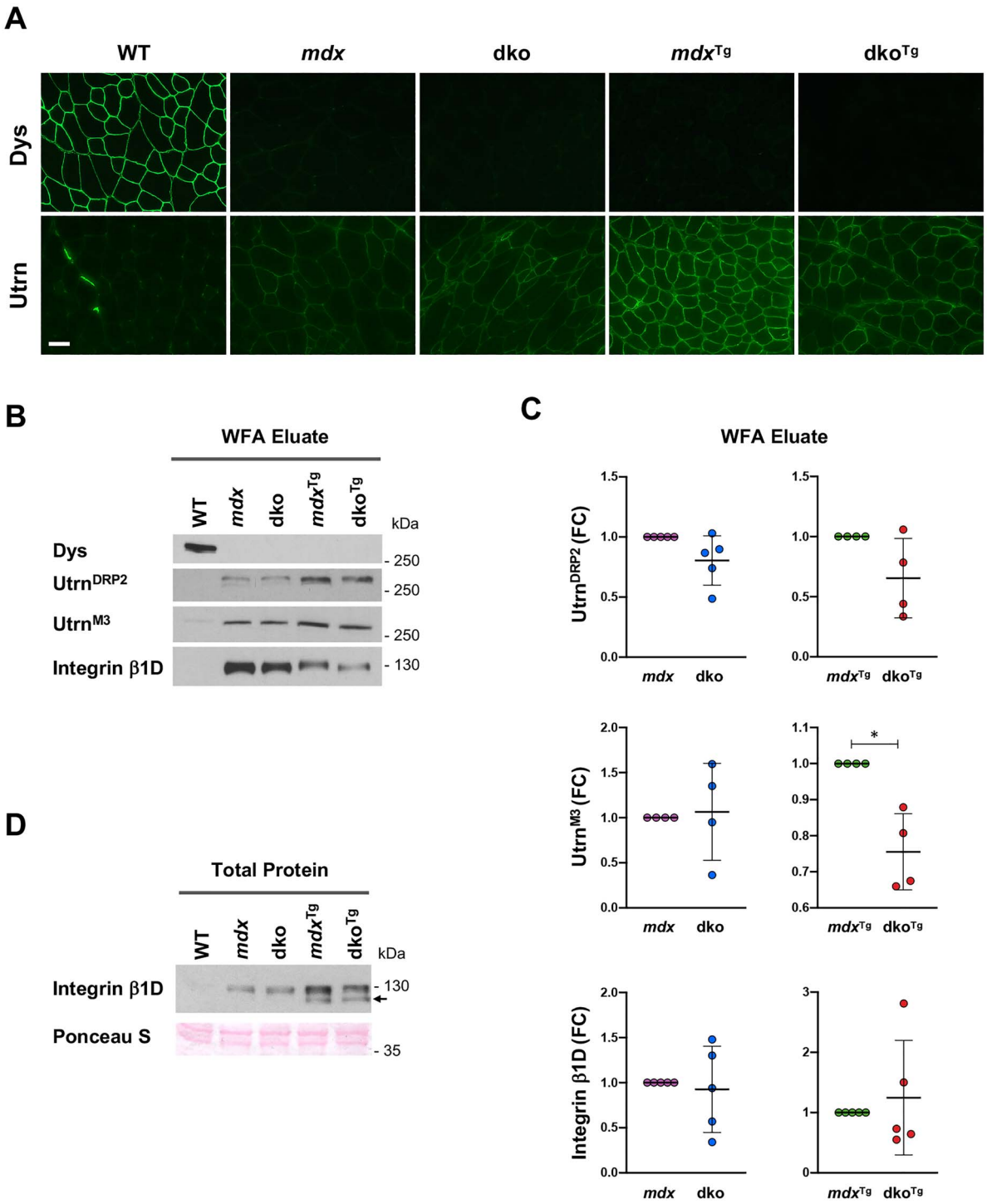

Figure 4. Partial restoration of sarcospan mediated upregulation of utrophin in the absence of GALGT2. (**A**) Immunofluorescence analysis of transverse quadriceps cryosections of WT, *mdx*, *mdx*:*Galgt2*$^{-/-}$ (dko), *mdx*:SSPN-Tg (*mdx*^{Tg}), and *mdx*:*Galgt2*$^{-/-}$:SSPN-Tg (dko^{Tg}) with antibodies against dystrophin (Dys) and utrophin (Utrn). Scale bar, 50 μm. (**B**) Skeletal muscle lysates enriched with WFA immunoblotted for dystrophin, utrophin (with two independent antibodies), and integrin β1D with quantification of data by densitometry in (**C**) with fold change (FC) shown for dko relative to *mdx* and dko^{Tg} relative to *mdx*^{Tg}. All data represented as mean +/− standard deviation. Statistical analysis was performed using Welch's *t*-test ($n = 4$–5 biological replicates per genotype; $^{*}P < 0.05$). (D) Total skeletal muscle homogenates immunoblotted with integrin β1D antibodies and Ponceau S is shown to demonstrate equal protein loading. Arrow marks precursor protein.

complexes, we used a mild detergent, digitonin, which captures specific, yet lower affinity interactions, with lectin that may be lost in a more stringent detergent. Solubilization with a modified RIPA buffer containing ionic detergents also did not affect the relative levels of WFA reactive α-DG ^{IIH6} enriched from *mdx* and dko quadricep muscles. Thus, differential protein extraction in NP-40 previously and digitonin or RIPA buffer here may account for experimental differences, as may the muscle studied (total

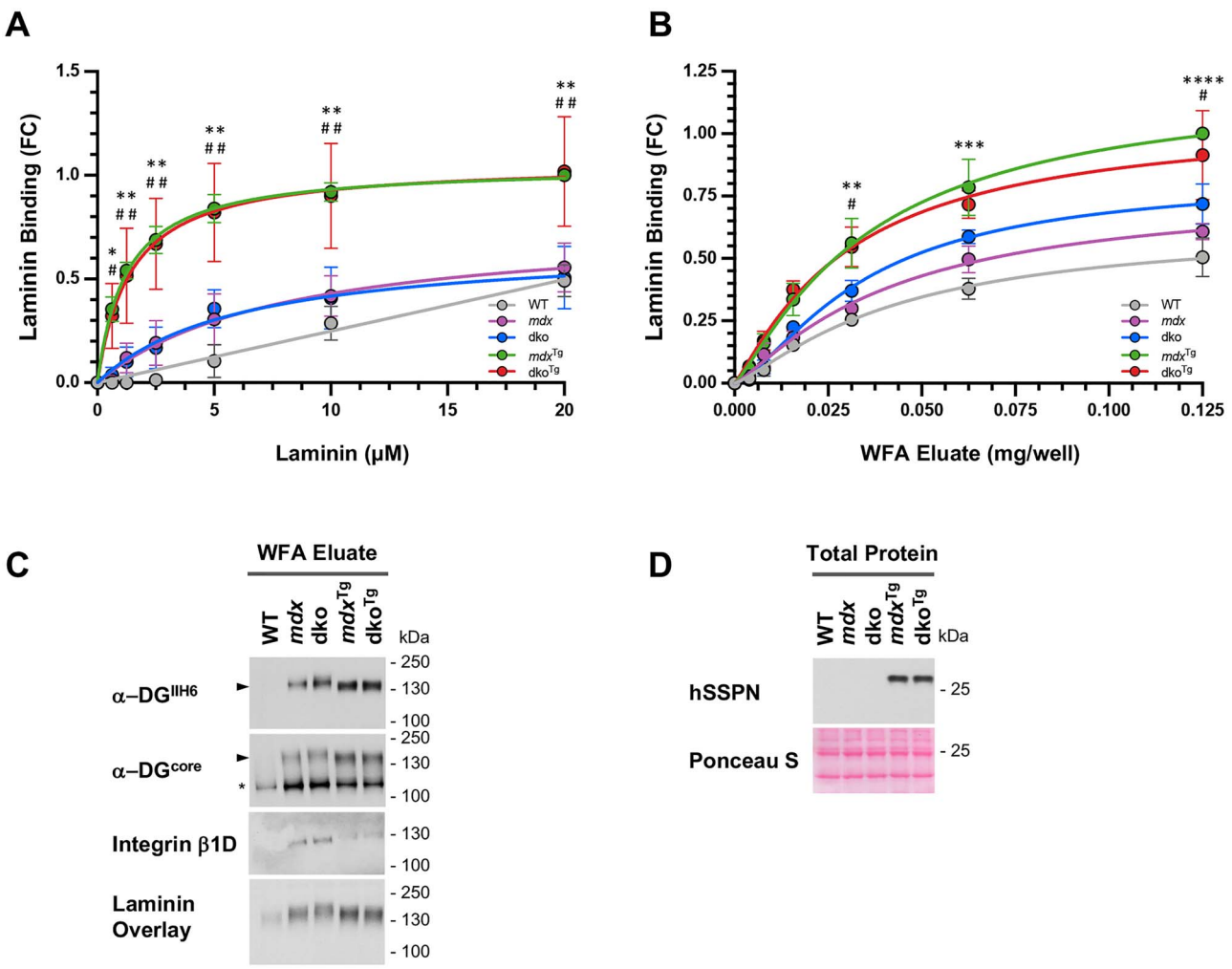

Figure 5. SSPN enhances the laminin-binding capacity in the absence of GALGT2. (**A**) Solid-phase laminin-binding assay to immobilized quadricep lysates enriched with WFA from 30–33-week-old WT, *mdx*, *mdx:Galgt2*$^{-/-}$ (dko), *mdx*:SSPN-Tg (*mdx*^{Tg}), and *mdx:Galgt2*$^{-/-}$:SSPN-Tg (dko^{Tg}). (**B**) Solid-phase α-DG binding assay to laminin-111 immobilized onto microtiter plates (**C**) Quadricep muscle lysates enriched with WFA immunoblotted with antibodies against laminin-binding glycoepitope of α-dystroglycan (α-DG^{IIH6}), the polypeptide protein core of α-dystroglycan (α-DG^{core}), or integrin β1D and laminin overlay. (**D**) Total quadriceps lysates probed with antibodies against human sarcospan (hSSPN) and Ponceau S shown to demonstrate equal protein loading. Arrowhead indicates mature glycosylated form of α-DG^{IIH6} and asterisk ($*$) denotes hypoglycosylated band. All data represented as mean +/− SEM fold change (FC) relative to *mdx*^{Tg}. Data are from $n = 3$ using identical WFA enrichments for all experiments. Statistical analysis was performed using two-way ANOVA with multiple comparison test ($*$, # $P < 0.05$, $**$, # # $P < 0.01$, $***P < 0.001$ and $****P < 0.0001$; $*$ indicates comparisons between *mdx and mdx*^{Tg}; # denotes comparisons between dko and dko^{Tg}).

skeletal muscle composed of hind and fore limbs muscles and quadriceps vs. gastrocnemius in the Xu *et al.* report).

Loss of GALGT2 did not alter the expression of any of the adhesion complex members analyzed in dko^{Tg} muscle with the exception of reduced utrophin at the sarcolemma with a concomitant trend for reduced incorporation in WFA enrichments. We have previously shown that genetic introduction of SSPN was unable to decrease disease severity in *mdx*:utrn$^{-/-}$ mice (Fig. 6D) (48). However, we did not observe any overt differences in the common histopathological phenotypes associated with *mdx* in dko^{Tg}. Furthermore, muscle integrity was maintained, which is important as membrane rupture is an initiating event in DMD suggesting that these levels of utrophin at the myofiber sarcolemma are sufficient.

How can SSPN overexpression enhance both the N-linked glycan on β-DG and the O-mannosyl chain of α-DG? Computational analysis predicts that SSPN shares similarities with the CD20 and tetraspanin protein families (17,54,55). Analogous to tetraspanins, as a molecular chaperone, SSPN may stabilize the DG heterodimer in the ER/Golgi compartments, alter the pH environment, or slow the transit kinetics providing sufficient time for improved maturation. It is also possible that SSPN may stabilize the interaction of glycotransferases or additional protein chaperones with the DGs. Furthermore, improved glycosylation may contribute to increased stability and deposition to the membrane (56,57). Consistent with its function as a protein scaffold, we show that SSPN influences the maturation and regulation of ITGB1.

We show that SSPN reduces the association of ITGB1 with DG complexes suggesting that SSPN alters the cross-talk between these two major adhesion complexes. Integrins and α-DG work together at the sarcolemma where they exhibit overlapping yet distinct functions to maintain adhesion and cellular signaling. In the *Large*^{myd} mice, overexpression of SSPN was unable to improve pathology, despite the presence of dystrophin and the endogenous upregulation of utrophin, and integrin (21). These

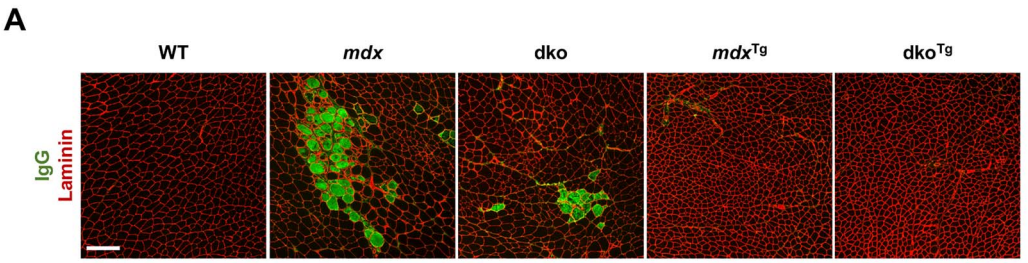

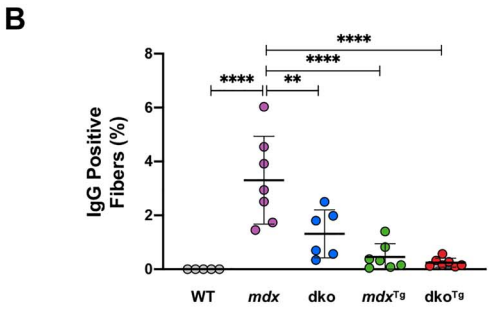

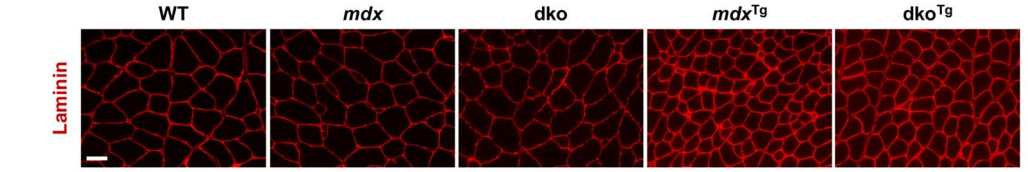

D

Table 1. SSPN ameliorates muscular dystrophy in a utrophin, α7 integrin-dependent, and mature α-dystroglycan manner.

	SSPN-Tg mice crossed with:				
Genotypes:	*mdx* mice (dystrophin-deficient mice)	*utrn*$^{-/-}$:*mdx* mice (utrophin and dystrophin double null mice)	*Itga*:*mdx* mice (α7 integrin and dystrophin double null mice)	*Galgt2*$^{-/-}$:*mdx* mice (GALGT2 and dystrophin double null mice)	*myd* mice (LARGE-deficient mice; model of CMD)
Question:	Does SSPN rescue cardiac, respiratory, and cardiac disease in the DMD murine model?	Is utrophin required for SSPN 'rescue' of *mdx*?	Is α7 integrin required for SSPN 'rescue' of *mdx*?	Is GALGT2 required for SSPN 'rescue' of *mdx*?	Is LARGE required for SSPN 'rescue' of *mdx*? The LARGE gene encodes a putative GlcNAc glycosyl-transferase that modifies α-DG.
Outcome:	Yes. SSPN reduces membrane instability, prevents degeneration/ regeneration cycles, and reduces fibrosis [21, 22, 24].	Yes. Utrophin is required for SSPN rescue of mdx [48]. SSPN-Tg failed to address central nucleation or muscle membrane damage in the double-null muscle.	Yes. Integrin α7 is required for SSPN rescue of mdx [48]. SSPN-Tg failed to address central nucleation or muscle membrane damage in the double-null muscle.	No. GALGT2 is not required for SSPN rescue of *mdx*. SSPN-Tg prevented muscle degeneration and damage to in the double-null muscle (This report).	Yes. SSPN is unable to compensate for loss of large activity [21], which is required for matriglycan modification of α-DG.

Figure 6. Sarcospan strengthens the sarcolemma in *mdx* muscle regardless of GALGT2 expression. (**A**) Representative images from immunofluorescence staining of mouse IgG antibodies (green) and laminin (red) to denote individual muscle fibers in transverse quadriceps cryosections from WT, *mdx*, *mdx*:*Galgt2*$^{-/-}$ (dko), *mdx*:SSPN-Tg (*mdx*^{Tg}) and *mdx*:*Galgt2*$^{-/-}$:SSPN-Tg (dko^{Tg}). Scale bar, 250 μm. (**B**) Quantification of percent IgG positive fibers from data in A. Data represented as mean +/− standard deviation. Statistical analysis was performed by one-way ANOVA with Tukey's multiple comparison tests ($n = 6$–7 quadriceps per genotype from 5 to 6 mice; $^{**}P < 0.01$ $^{***}P < 0.001$). (**C**) Representative higher magnification of laminin expression in transverse quadricep sections. Scale bar, 50 μm. (**D**) Table summarizing the findings from our group revealing that SSPN amelioration of pathology in the dystrophin-deficient mice requires utrophin, integrin $\alpha 7$ and LARGE 1 (critical for proper maturation of α-DG).

molecular changes were unable to compensate for disease indicating that mature glycosylated α-DG ^{IIH6} decorated with the laminin-binding epitope matriglycan may be required for SSPN-mediated rescue of muscle pathology. Combined with our previous findings, although overexpression of SSPN increased both the matriglycan and CT2 glycan carbohydrate modifications on α-DG, loss of GALGT2 activity has no effect on SSPN-mediated improvements in *mdx* disease. These data reveal

that the matriglycan modification, and not the CT2 glycan, is necessary for SSPN to ameliorate dystrophy.

Our data suggest that SSPN is mediating its effects by elevating WFA reactive α-DG^{IIH6} complexes at the extrasynaptic sarcolemma in dystrophin-deficient muscle. We show that transgenic overexpression of SSPN elevates the levels of WFA reactive mature α-DG^{IIH6} specifically by promoting matriglycan glycosylation, which in turn leads to increased laminin-binding capacity. Interestingly, this also correlates with the concomitant increase of one of its major binding partners, laminin, at the ECM. It is possible that the hyperglycosylated glycoform of α-DG^{IIH6} may simultaneously bind to multiple matrix ligands. The matriglycan epitope on α-DG is capable of binding to the LG domains on several matrix proteins in addition to laminin, including agrin and perlecan in muscle. In contrast, the interaction with biglycan is independent of sugar residues on α-DG and is upregulated in *mdx* (58). We have previously observed modest increases in agrin (above levels in *mdx*) and dramatically elevated levels of plectin in homogenates from *mdx*:SSPN-Tg muscle (21). Through distinct binding motifs, plectin connects the cytoskeleton to the cell membrane by simultaneously associating with multiple proteins such as F-actin, β-DG, dystrophin, utrophin and integrin (59). Transgenic introduction of SSPN may serve to re-wire the cell to matrix connections by strengthening the cellular adhesion and signaling, which in turn increases the resilience of the myofiber membrane.

Materials and Methods

Animal models

C57BL/6 J wild-type and *mdx* mice were obtained from Jackson Laboratories (Bar Harbor, ME). Generation of transgenic (Tg) mice harboring the full-length human SSPN cDNA have been previous described (20,21). *Galgt2* null mice were a generous gift from Dr Paul Martin (The Research Institute at Children's Nationwide Hospital; (29)). *mdx*:*Galgt2*$^{-/-}$:SSPN-Tg mice were created by breeding *mdx*:*Gaglt2*$^{+/-}$:SSPN-Tg to *mdx*:*Gaglt2*$^{+/-}$:SSPN-non-Tg (Fig. 1A). Male progeny 30–33 weeks old were used for the laminin-binding assay and all data generated in Figure 5. Male mice 10–13 weeks old were used for all remaining experiments. Mice were maintained in the Life Sciences Vivarium at the University of California, Los Angeles according to approved protocols and guidelines by the UCLA Institutional Animal Care and Use Committee.

Antibodies

Dystrophin (MANDYS1 3B7; Development Studies Hybridoma Bank); Utrophin^{DRP2} (DRP2-cE; Leica Biosystems); Utrophin^{M3} (MANCHO3 84A; Development Studies Hybridoma Bank); α-DG^{IIH6} (C4s; Development Studies Hybridoma Bank); α-DG Core 45-3 was a kind gift from Aaron Beedle (SUNY Binghamton University, ab199768; Abcam) (60); β-DG (MANDAG2 7D11; Development Studies Hybridoma Bank); α-SG (EPR14773; Abcam); β-SG (NCL-L-b-SARC; Leica Biosystems); δ-SG (EPR8706; Abcam); γ-SG (GTX117176; GeneTex); hSSPN (LS-C747357; LifeSpan Biosciences); SSPN E2 (sc-393 187; Santa Cruz Biotechnology); β1D-Integrin (MAB1900; Millipore); laminin (L9393; Sigma-Aldrich); eMHC (F1.652; Development Studies Hybridoma Bank); Biotinylated anti-rabbit (BA-1000; Vector Laboratories); Pax7 (AB 528428 l; Development Studies Hybridoma Bank); Biotinylated anti-mouse (BA-9200; Vector Laboratories), Laminin (23 017 015; Thermo Scientific).

Immunohistochemistry

Tissue was frozen in liquid nitrogen cooled isopentane and mounted on OCT (Tissue-Tek) and stored at −80°C. To inhibit non-specific interactions, transverse cryosections (7 μm thick) were blocked with 3% BSA at room temperature, followed by incubation with avidin/biotin blocking kit (Vector Laboratories) and finally a Mouse on Mouse blocking (M.O.M; Vector Laboratories) step was performed for antibodies were raised in mouse. Antibodies or biotinylated lectin WFA (4 μg/ml; Vector Laboratories) were allowed to bind overnight at 4°C in either 3% BSA or M.O.M block. Sections were washed with PBS and primary antibodies were detected with species specific biotinylated antibodies for 1 hour at room temperature. Bound antibodies were visualized by incubation with fluorescein-conjugated Avidin D (Vector Laboratories). Slides were wet mounted in Vectashield with or without DAPI (Vector Laboratories) before analysis by microscopy on Zeiss Axio Observer 7 or Axio Imager M2 (Carl Zeiss). M.O.M block was omitted for mouse IgG immunostaining to assess membrane permeability. Images were captured with Hammatsu ORCA-Flash 4.0 V3 digital complementary metal oxide semiconductor camera and either EC Plan-Neofluar 10×/0.30 Ph1 or Plan-Aprochromat 20×/0.8 M27 objectives. All measurements were performed using Image J software (NIH) or Zen (Carl Zeiss). Percent of IgG uptake was determined by counting IgG-positive fibers with clear laminin boundary and dividing by the total number of myofibers. Percent eMHC positive fibers and Pax7 positive fibers were similarly quantified. Cross-sectional area was determined by marking the perimeter of myofibers using a macro (a kind gift form Karen Christman, UCSD) to Image J (NIH). Each individual myofiber was checked and corrected manually to ensure correct myofiber bounder was marked. Data were binned per 500 μm^2 and values greater than 8500 μm^2 were excluded due to very low counts. Prism software (GraphPad) was used to plot graphs and perform statistical analysis as stated in figure legends.

Histology

Transverse cryosections 7 μm thick on slides were acclimated at RT for 15 min, incubated with hematoxylin (5 min), rinsed with ddH_2O, stained with eosin (5 min), and dehydrated in a series of ethanol rinses of 70, 80, 90 and 100% before final incubation in xylene. Slides were mounted in Permount and allowed to harden overnight. Tissues were imaged by epifluorescence microscopy on Zeiss Axio Observer 7 or Axio Imager M2 with Axiocam 506 color digital camera (Carl Zeiss) and either EC Plan-Neofluar 10×/0.30 M27 or Plan-Apochromat 20×/0.8 M27 objectives. Percent central nucleation was assessed by counting fibers with centrally placed nuclei relative to total number of fibers per transverse section. Prism software (GraphPad) was used to plot data and perform statistical analysis specified in the figure legends.

Lectin protein enrichment assay

Total skeletal muscle (composed of all hindlimbs and forelimbs muscles and excluding quadriceps, which were used for immunofluorescence analysis) snap frozen in liquid nitrogen and stored at −80°C were ground to fine powder using a biopulverizer mortar and pestle. Ground tissue was dounce homogenized in digitonin lysis buffer (50 mM Tris, 500 mM NaCl, 1% digitonin pH 7.8) with Halt protease and phosphatase inhibitors (Pierce) and rotated for 2 hour at 4°C. Insoluble matter

was sediment by centrifuging at 15 000 × g for 20 min at 4°C, and the clarified lysate was transferred into a new tube. Protein concentration was determined with the DC Protein Assay (Bio Rad). Adhesion complex was batch extracted by incubation of 20 mg homogenates with 1 mL agarose bound lectins WFA or sWGA (Vector Laboratories) and rotated overnight at 4°C. After spinning at 4000 × g for 5 min, the supernatant was saved as the void fraction and the agarose beads were washed five times with wash buffer containing protease inhibitors (50 mM Tris, 500 mM NaCl, 0.1% digitonin, 0.2 mM PMSF, 0.75 mM benzamadine, 5μM calpain I and 5μm calpain II). Bound proteins were eluted with 0.3 M GalNac (N-acetyl-D-galactosamine; Carbosynth) for WFA or 0.3 mM GlcNAc (N-acetyl glucosamine; Sigma-Aldrich) for sWGA-conjugated beads in elution buffer (50 mM Tris, 500 mM NaCl, 0.1% digitonin, 0.2 mM PMSF, 0.75 mM benzamadine, 5 μM calpain I and 5 μm Calpain II) and concentrated using Amicon Ultra-15 10 kDa filtration columns (Millipore). All centrifugation steps were performed at 4°C. All fractions (total protein, void, washes, eluates) were stored at −80°C until analyzed.

Solid-phase binding assay

Quadriceps muscles frozen in liquid nitrogen cooled isopentane mounted on OCT (Tissue-Tek) and stored at −80°C were ground to fine powder using a biopulverizer mortar and pestle. Ground tissue was dounce homogenized in a modified RIPA lysis buffer (50 mM Tris, 500 mM NaCl, 1% TX-100, 0.5% sodium deoxycholate, 0.1% SDS pH 7.8) with Halt protease and phosphatase inhibitors (Pierce) and rotated for 2 hour at 4°C. Lysates were clarified by centrifuging and protein concentration was determined. After adjusting salt concentration to 150 mM with modified RIPA, adhesion complex was batch extracted by incubating 10 mg homogenates with 0.5 mL agarose bound lectins WFA (Vector Laboratories) as described above with the following modifications. Washes and elutions were performed with lectin wash buffer (50 mM Tris, 150 mM NaCl, 0.1% TX-100, pH 7.8). For laminin-binding solid-phase assay, 96-well Nunc MaxiSorp plates (Invitrogen) were coated with 100 μl of WFA enrichment overnight at 4°C in bicarbonate buffer. All subsequent steps were performed at room temperature. After three washes with 0.5% BSA in LBB (10 mM triethanolamine, 140 mM NaCl, 1 mM $CaCl_2$, 1 mM $MgCl_2$, pH 7.6), wells were blocked with 3% BSA in LBB for two hours, washed again before incubation with varying concentration of laminin in 3% BSA in LBB for another two hours. After washing away unbound laminin, wells were probed with anti-laminin antibodies (L9393; Sigma Aldrich) for one hour and washed before addition of HRP-conjugated goat anti-Rabbit IgG (Abcam) for another hour. Unbound antibodies were washed away and signal developed using tetramethylbenzidine (Thermo Scientific). Absorbance was measure at 652 nM using a Spectramax M2 microplate reader (Molecular Devices). For solid-phase α-DG binding assay, 2 μg/ml laminin in bicarbonate buffer was coated overnight at 4°C. After washing with LBB and subsequent blocking for 1 hour, wells were incubated with various concentration of WFA enrichments (mg/ml equivalent to input used for lectin enrichments) in blocking buffer overnight at 4°C. The next day, wells were washed, probed with antibodies to α-DG core polypeptide (Abcam) and subsequently HRP-conjugated goat anti-Rabbit IgG (Abcam) before developing with tetramethylbenzidine (Thermo Scientific). The reaction was stopped with 2 M sulfuric acid and absorbance read at 450 nM. Prism software (GraphPad) was used to plot data, curve fitting and perform statistical analysis specified in the figure legends. Negative points were converted to zero, and data are reported as fold change relative to *mdx*^{Tg}.

Immunoblotting

Twenty micrograms of total protein fractions or equimolar amounts of eluates were separated by SDS-PAGE on 4–12% gradient Bolt Bis-Tris gels (Thermo Scientific), then transferred onto nitrocellulose membraned (Millipore). PageRuler Plus Prestained Protein Ladder (Thermo Scientific) was used as a molecular weight marker. Western blotting and laminin overlays were performed as previously described (21). Briefly, nitrocellulose membranes blocked with 5% non-fat dry milk (Carnation) in TBST followed by primary antibody incubation overnight at 4°C with gentle rotation. Membranes were extensively rinsed in TBST before applying secondary antibody horseradish peroxidase-conjugated anti-mouse or anti-rabbit IgG (Abcam) or IgM (Thermo Scientific). For laminin overlay assays, membranes were blocked in 5% non-fat dry milk in LBB before incubation in 0.5 μg/ml laminin in 3% BSA LBB overnight at 4°C. The next day, membranes were washed and probed with anti-laminin antibodies (L9393; Sigma Aldrich) followed by detection with horseradish peroxidase-conjugated anti-rabbit IgG. Bound antibodies were detected with SuperSignal West Pico Plus Chemiluminescence (Thermo Scientific) on GeneMate Blue Autoradiography Film (GeneMate). Densitometry measurements were performed with Image J software (NIH). Where needed, multiple films were assessed by densitometry to determine saturation point and ensure band intensity did not reach saturation. Since SSPN-Tg samples display band intensities many fold greater than non-transgenic samples, data for dko were normalized to *mdx* and dko^{Tg} were normalized to *mdx*^{Tg} to prevent saturation. Similarly, since wild-type samples contain low levels of WFA bound protein relative to dystrophin-deficient samples, it was not possible to quantify band intensities for wild-type without saturation of remaining samples. Data were plotted and statistical analysis performed on Prism software (GraphPad) as described in the figure legends. Post hoc power analysis was performed using G power 3.1 (61).

Authors' Contributions

H.M. designed and performed experiments, analyzed all data, prepared all figures, and wrote the manuscript. R.L.S. performed cryosectioning, immunohistochemistry and central nucleation counts, fiber counting, and CSA measurements under the supervision of H.M. K.M.S. performed cryosectioning, immunohistochemistry, central nucleation counts, and Pax7 positive cell counts. A.M.B. provided α-DG Core 45–3 antibodies. R.H.C. conceived of the project and consulted on all experiments, data analysis, and manuscript preparation. All authors reviewed and edited the manuscript.

Supplementary Material

Supplementary Material is available at *HMG* online.

Acknowledgements

We are grateful to Sarah Overington for fiber counting, Shuxin Wen, Dr Melissa Spencer, and members of the Crosbie Lab for

technical assistance and mouse tissue collection. We thank Dr Paul T. Martin (Nationwide Children's Hospital) for his expertise and generously providing the *mdx:Galgt2* $^{-/-}$ mice, which were critical to this study. We thank Dr Karen Christman (University of California, San Diego) for sharing a macro add-on to Image J to measure fiber diameter. We thank Devin Gibbs, Kholoud Saleh and Dr April Pyle (University of California, Los Angeles) for Pax7 immunostaining protocol.

Conflict of Interest statement. The authors declare no competing conflict of interest.

Funding

The work was supported by the Boyer family Scholarship through the UCLA Undergraduate Research Fellows Program [to R.L.S.], the J.W. and Nellie MacDowall Scholarship through the UCLA Undergraduate Research Scholars Program [to R.L.S], National Institutes of Health [NIGMS R01 GM111939 to A.M.B., NIAMS R01 AR048179 to R.H.C. and NHLBI R01 HL126204 to R.H.C.].

References

1. Hoffman, E.P., Brown, R.H., Jr. and Kunkel, L.M. (1987) Dystrophin: the protein product of the Duchenne muscular dystrophy locus. *Cell*, **51**, 919–928.
2. Mendell, J.R., Shilling, C., Leslie, N.D., Flanigan, K.M., Al-Dahhak, R., Gastier-Foster, J., Kneile, K., Dunn, D.M., Duval, B., Aoyagi, A. *et al.* (2012) Evidence-based path to newborn screening for Duchenne muscular dystrophy. *Ann. Neurol.*, **71**, 304–313.
3. Ervasti, J.M. and Campbell, K.P. (1991) Membrane organization of the dystrophin-glycoprotein complex. *Cell*, **66**, 1121–1131.
4. Campbell, K.P. and Kahl, S.D. (1989) Association of dystrophin and an integral membrane glycoprotein. *Nature*, **338**, 259–262.
5. Ervasti, J.M., Ohlendieck, K., Kahl, S.D., Gaver, M.G. and Campbell, K.P. (1990) Deficiency of a glycoprotein component of the dystrophin complex in dystrophic muscle. *Nature*, **345**, 315–319.
6. Ervasti, J.M., Kahl, S.D. and Campbell, K.P. (1991) Purification of dystrophin from skeletal muscle. *J. Biol. Chem.*, **266**, 9161–9165.
7. Yoshida, M. and Ozawa, E. (1990) Glycoprotein complex anchoring dystrophin to sarcolemma. *J. Biochem.*, **108**, 748–752.
8. Ervasti, J.M. and Campbell, K.P. (1993) A role for the dystrophin-glycoprotein complex as a transmembrane linker between laminin and actin. *J. Cell Biol.*, **122**, 809–823.
9. Weller, B., Karpati, G. and Carpenter, S. (1990) Dystrophin-deficient mdx muscle fibers are preferentially vulnerable to necrosis induced by experimental lengthening contractions. *J. Neurol. Sci.*, **100**, 9–13.
10. Petrof, B.J., Shrager, J.B., Stedman, H.H., Kelly, A.M. and Sweeney, H.L. (1993) Dystrophin protects the sarcolemma from stresses developed during muscle contraction. *Proc. Natl. Acad. Sci. U. S. A.*, **90**, 3710–3714.
11. Matsumura, K., Ervasti, J.M., Ohlendieck, K., Kahl, S.D. and Campbell, K.P. (1992) Association of dystrophin-related protein with dystrophin-associated proteins in mdx mouse muscle. *Nature*, **360**, 588–591.
12. Tinsley, J.M., Potter, A.C., Phelps, S.R., Fisher, R., Trickett, J.I. and Davies, K.E. (1996) Amelioration of the dystrophic phenotype of mdx mice using a truncated utrophin transgene. *Nature*, **384**, 349–353.
13. Deconinck, N., Tinsley, J., De Backer, F., Fisher, R., Kahn, D., Phelps, S., Davies, K. and Gillis, J.M. (1997) Expression of truncated utrophin leads to major functional improvements in dystrophin-deficient muscles of mice. *Nat. Med.*, **3**, 1216–1221.
14. Rafael, J.A., Tinsley, J.M., Potter, A.C., Deconinck, A.E. and Davies, K.E. (1998) Skeletal muscle-specific expression of a utrophin transgene rescues utrophin-dystrophin deficient mice. *Nat. Genet.*, **19**, 79–82.
15. Pearce, M., Blake, D.J., Tinsley, J.M., Byth, B.C., Campbell, L., Monaco, A.P. and Davies, K.E. (1993) The utrophin and dystrophin genes share similarities in genomic structure. *Hum. Mol. Genet.*, **2**, 1765–1772.
16. Tinsley, J.M., Blake, D.J., Roche, A., Fairbrother, U., Riss, J., Byth, B.C., Knight, A.E., Kendrick-Jones, J., Suthers, G.K., Love, D.R. *et al.* (1992) Primary structure of dystrophin-related protein. *Nature*, **360**, 591–593.
17. Crosbie, R.H., Heighway, J., Venzke, D.P., Lee, J.C. and Campbell, K.P. (1997) Sarcospan, the 25-kDa transmembrane component of the dystrophin-glycoprotein complex. *J. Biol. Chem.*, **272**, 31221–31224.
18. Crosbie, R.H., Lebakken, C.S., Holt, K.H., Venzke, D.P., Straub, V., Lee, J.C., Grady, R.M., Chamberlain, J.S., Sanes, J.R. and Campbell, K.P. (1999) Membrane targeting and stabilization of sarcospan is mediated by the sarcoglycan subcomplex. *J. Cell Biol.*, **145**, 153–165.
19. Crosbie, R.H., Lim, L.E., Moore, S.A., Hirano, M., Hays, A.P., Maybaum, S.W., Collin, H., Dovico, S.A., Stolle, C.A., Fardeau, M. *et al.* (2000) Molecular and genetic characterization of sarcospan: insights into sarcoglycan-sarcospan interactions. *Hum. Mol. Genet.*, **9**, 2019–2027.
20. Peter, A.K., Marshall, J.L. and Crosbie, R.H. (2008) Sarcospan reduces dystrophic pathology: stabilization of the utrophin-glycoprotein complex. *J. Cell Biol.*, **183**, 419–427.
21. Marshall, J.L., Holmberg, J., Chou, E., Ocampo, A.C., Oh, J., Lee, J., Peter, A.K., Martin, P.T. and Crosbie-Watson, R.H. (2012) Sarcospan-dependent Akt activation is required for utrophin expression and muscle regeneration. *J. Cell Biol.*, **197**, 1009–1027.
22. Gibbs, E.M., Marshall, J.L., Ma, E., Nguyen, T.M., Hong, G., Lam, J.S., Spencer, M.J. and Crosbie-Watson, R.H. (2016) High levels of sarcospan are well tolerated and act as a sarcolemmal stabilizer to address skeletal muscle and pulmonary dysfunction in DMD. *Hum. Mol. Genet.*, **25**, 5395–5406.
23. Parvatiyar, M.S., Brownstein, A.J., Kanashiro-Takeuchi, R.M., Collado, J.R., Dieseldorff Jones, K.M., Gopal, J., Hammond, K.G., Marshall, J.L., Ferrel, A., Beedle, A.M. *et al.* (2019) Stabilization of the cardiac sarcolemma by sarcospan rescues DMD-associated cardiomyopathy. *JCI Insight*, 5, e123855.
24. Parvatiyar, M.S., Marshall, J.L., Nguyen, R.T., Jordan, M.C., Richardson, V.A., Roos, K.P. and Crosbie-Watson, R.H. (2015) Sarcospan regulates cardiac isoproterenol response and prevents Duchenne muscular dystrophy-associated cardiomyopathy. *J. Am. Heart Assoc.*, 4, e002481.
25. Xia, B., Hoyte, K., Kammesheidt, A., Deerinck, T., Ellisman, M. and Martin, P.T. (2002) Overexpression of the CT GalNAc transferase in skeletal muscle alters myofiber growth, neuromuscular structure, and laminin expression. *Dev. Biol.*, **242**, 58–73.

26. Nguyen, H.H., Jayasinha, V., Xia, B., Hoyte, K. and Martin, P.T. (2002) Overexpression of the cytotoxic T cell GalNAc transferase in skeletal muscle inhibits muscular dystrophy in mdx mice. *Proc. Natl. Acad. Sci. U. S. A.*, **99**, 5616–5621.
27. Martin, P.T., Xu, R., Rodino-Klapac, L.R., Oglesbay, E., Camboni, M., Montgomery, C.L., Shontz, K., Chicoine, L.G., Clark, K.R., Sahenk, Z. *et al.* (2009) Overexpression of Galgt2 in skeletal muscle prevents injury resulting from eccentric contractions in both mdx and wild-type mice. *Am. J. Physiol. Cell Physiol.*, **296**, C476–C488.
28. Smith, P.L. and Lowe, J.B. (1994) Molecular cloning of a murine N-acetylgalactosamine transferase cDNA that determines expression of the T lymphocyte-specific CT oligosaccharide differentiation antigen. *J. Biol. Chem.*, **269**, 15162–15171.
29. Xu, R., Singhal, N., Serinagaoglu, Y., Chandrasekharan, K., Joshi, M., Bauer, J.A., Janssen, P.M. and Martin, P.T. (2015) Deletion of Galgt2 (B4Galnt2) reduces muscle growth in response to acute injury and increases muscle inflammation and pathology in dystrophin-deficient mice. *Am. J. Pathol.*, **185**, 2668–2684.
30. Yoon, J.H., Chandrasekharan, K., Xu, R., Glass, M., Singhal, N. and Martin, P.T. (2009) The synaptic CT carbohydrate modulates binding and expression of extracellular matrix proteins in skeletal muscle: partial dependence on utrophin. *Mol. Cell. Neurosci.*, **41**, 448–463.
31. Connolly, A.M., Keeling, R.M., Mehta, S., Pestronk, A. and Sanes, J.R. (2001) Three mouse models of muscular dystrophy: the natural history of strength and fatigue in dystrophin-, dystrophin/utrophin-, and laminin alpha2-deficient mice. *Neuromuscul. Disord.*, **11**, 703–712.
32. Kornegay, J.N., Childers, M.K., Bogan, D.J., Bogan, J.R., Nghiem, P., Wang, J., Fan, Z., Howard, J.F., Jr., Schatzberg, S.J., Dow, J.L. *et al.* (2012) The paradox of muscle hypertrophy in muscular dystrophy. *Phys. Med. Rehabil. Clin. N. Am.*, **23**, 149, xii–172.
33. Yoshida-Moriguchi, T., Yu, L., Stalnaker, S.H., Davis, S., Kunz, S., Madson, M., Oldstone, M.B., Schachter, H., Wells, L. and Campbell, K.P. (2010) O-mannosyl phosphorylation of alpha-dystroglycan is required for laminin binding. *Science*, **327**, 88–92.
34. Yoshida-Moriguchi, T. and Campbell, K.P. (2015) Matriglycan: a novel polysaccharide that links dystroglycan to the basement membrane. *Glycobiology*, **25**, 702–713.
35. Praissman, J.L., Willer, T., Sheikh, M.O., Toi, A., Chitayat, D., Lin, Y.Y., Lee, H., Stalnaker, S.H., Wang, S., Prabhakar, P.K. *et al.* (2016) The functional O-mannose glycan on alpha-dystroglycan contains a phospho-ribitol primed for matriglycan addition. *elife*, 5, e14473.
36. Michele, D.E., Barresi, R., Kanagawa, M., Saito, F., Cohn, R.D., Satz, J.S., Dollar, J., Nishino, I., Kelley, R.I., Somer, H. *et al.* (2002) Post-translational disruption of dystroglycan-ligand interactions in congenital muscular dystrophies. *Nature*, **418**, 417–422.
37. Kanagawa, M., Saito, F., Kunz, S., Yoshida-Moriguchi, T., Barresi, R., Kobayashi, Y.M., Muschler, J., Dumanski, J.P., Michele, D.E., Oldstone, M.B. *et al.* (2004) Molecular recognition by LARGE is essential for expression of functional dystroglycan. *Cell*, **117**, 953–964.
38. Durko, M., Allen, C., Nalbantoglu, J. and Karpati, G. (2010) CT-GalNAc transferase overexpression in adult mice is associated with extrasynaptic utrophin in skeletal muscle fibres. *J. Muscle Res. Cell Motil.*, **31**, 181–193.
39. Thomas, P.J., Xu, R. and Martin, P.T. (2016) B4GALNT2 (GALGT2) gene therapy reduces skeletal muscle pathology in the FKRP P448L mouse model of limb girdle muscular dystrophy 2I. *Am. J. Pathol.*, **186**, 2429–2448.
40. Zygmunt, D.A., Xu, R., Jia, Y., Ashbrook, A., Menke, C., Shao, G., Yoon, J.H., Hamilton, S., Pisharath, H., Bolon, B. *et al.* (2019) rAAVrh74.MCK.GALGT2 demonstrates safety and widespread muscle glycosylation after intravenous delivery in C57BL/6J mice. *Mol Ther Methods Clin Dev*, **15**, 305–319.
41. Xu, R., Jia, Y., Zygmunt, D.A. and Martin, P.T. (2019) rAAVrh74.MCK.GALGT2 protects against loss of hemodynamic function in the aging mdx mouse heart. *Mol. Ther.*, **27**, 636–649.
42. Ibraghimov-Beskrovnaya, O., Ervasti, J.M., Leveille, C.J., Slaughter, C.A., Sernett, S.W. and Campbell, K.P. (1992) Primary structure of dystrophin-associated glycoproteins linking dystrophin to the extracellular matrix. *Nature*, **355**, 696–702.
43. Jung, D., Yang, B., Meyer, J., Chamberlain, J.S. and Campbell, K.P. (1995) Identification and characterization of the dystrophin anchoring site on beta-dystroglycan. *J. Biol. Chem.*, **270**, 27305–27310.
44. Holt, K.H., Lim, L.E., Straub, V., Venzke, D.P., Duclos, F., Anderson, R.D., Davidson, B.L. and Campbell, K.P. (1998) Functional rescue of the sarcoglycan complex in the BIO 14.6 hamster using delta-sarcoglycan gene transfer. *Mol. Cell*, **1**, 841–848.
45. Miller, G., Wang, E.L., Nassar, K.L., Peter, A.K. and Crosbie, R.H. (2007) Structural and functional analysis of the sarcoglycan-sarcospan subcomplex. *Exp. Cell Res.*, **313**, 639–651.
46. Nguyen, T.M., Ellis, J.M., Love, D.R., Davies, K.E., Gatter, K.C., Dickson, G. and Morris, G.E. (1991) Localization of the DMDL gene-encoded dystrophin-related protein using a panel of nineteen monoclonal antibodies: presence at neuromuscular junctions, in the sarcolemma of dystrophic skeletal muscle, in vascular and other smooth muscles, and in proliferating brain cell lines. *J. Cell Biol.*, **115**, 1695–1700.
47. Zhao, J., Yoshioka, K., Miyatake, M. and Miike, T. (1992) Dystrophin and a dystrophin-related protein in intrafusal muscle fibers, and neuromuscular and myotendinous junctions. *Acta Neuropathol.*, **84**, 141–146.
48. Marshall, J.L., Oh, J., Chou, E., Lee, J.A., Holmberg, J., Burkin, D.J. and Crosbie-Watson, R.H. (2015) Sarcospan integration into laminin-binding adhesion complexes that ameliorate muscular dystrophy requires utrophin and alpha7 integrin. *Hum. Mol. Genet.*, **24**, 2011–2022.
49. Burkin, D.J., Wallace, G.Q., Nicol, K.J., Kaufman, D.J. and Kaufman, S.J. (2001) Enhanced expression of the alpha 7 beta 1 integrin reduces muscular dystrophy and restores viability in dystrophic mice. *J. Cell Biol.*, **152**, 1207–1218.
50. Liu, J., Milner, D.J., Boppart, M.D., Ross, R.S. and Kaufman, S.J. (2012) beta1D chain increases alpha7beta1 integrin and laminin and protects against sarcolemmal damage in mdx mice. *Hum. Mol. Genet.*, **21**, 1592–1603.
51. Straub, V., Rafael, J.A., Chamberlain, J.S. and Campbell, K.P. (1997) Animal models for muscular dystrophy show different patterns of sarcolemmal disruption. *J. Cell Biol.*, **139**, 375–385.
52. Burkin, D.J., Wallace, G.Q., Milner, D.J., Chaney, E.J., Mulligan, J.A. and Kaufman, S.J. (2005) Transgenic expression of {alpha}7{beta}1 integrin maintains muscle integrity, increases regenerative capacity, promotes hypertrophy, and reduces cardiomyopathy in dystrophic mice. *Am. J. Pathol.*, **166**, 253–263.

53. Shu, C., Kaxon-Rupp, A.N., Collado, J.R., Damoiseaux, R. and Crosbie, R.H. (2019) Development of a high-throughput screen to identify small molecule enhancers of sarcospan for the treatment of Duchenne muscular dystrophy. *Skelet. Muscle*, **9**, 32.
54. Marshall, J.L., Kwok, Y., McMorran, B.J., Baum, L.G. and Crosbie-Watson, R.H. (2013) The potential of sarcospan in adhesion complex replacement therapeutics for the treatment of muscular dystrophy. *FEBS J.*, **280**, 4210–4229.
55. Marshall, J.L. and Crosbie-Watson, R.H. (2013) Sarcospan: a small protein with large potential for Duchenne muscular dystrophy. *Skelet. Muscle*, **3**, 1.
56. Holt, K.H., Crosbie, R.H., Venzke, D.P. and Campbell, K.P. (2000) Biosynthesis of dystroglycan: processing of a precursor propeptide. *FEBS Lett.*, **468**, 79–83.
57. Esapa, C.T., Bentham, G.R., Schroder, J.E., Kroger, S. and Blake, D.J. (2003) The effects of post-translational processing on dystroglycan synthesis and trafficking. *FEBS Lett.*, **555**, 209–216.
58. Bowe, M.A., Mendis, D.B. and Fallon, J.R. (2000) The small leucine-rich repeat proteoglycan biglycan binds to alpha-dystroglycan and is upregulated in dystrophic muscle. *J. Cell Biol.*, **148**, 801–810.
59. Rezniczek, G.A., Konieczny, P., Nikolic, B., Reipert, S., Schneller, D., Abrahamsberg, C., Davies, K.E., Winder, S.J. and Wiche, G. (2007) Plectin 1f scaffolding at the sarcolemma of dystrophic (mdx) muscle fibers through multiple interactions with beta-dystroglycan. *J. Cell Biol.*, **176**, 965–977.
60. Fortunato, M.J., Ball, C.E., Hollinger, K., Patel, N.B., Modi, J.N., Rajasekaran, V., Nonneman, D.J., Ross, J.W., Kennedy, E.J., Selsby, J.T. *et al.* (2014) Development of rabbit monoclonal antibodies for detection of alpha-dystroglycan in normal and dystrophic tissue. *PLoS One*, **9**, e97567.
61. Faul, F., Erdfelder, E., Buchner, A. and Lang, A.G. (2009) Statistical power analyses using G*power 3.1: tests for correlation and regression analyses. *Behav. Res. Methods*, **41**, 1149–1160.